Optimization calculations for neutron production target at Variable Energy Cyclotron Centre, Kolkata with 50 MeV electron linear accelerator

Nisith Kr Das[1,*] and S. Chatterjee[2]

[1]Variable Energy Cyclotron Centre and
[2]Radiological Physics and Advisory Division, Bhabha Atomic Research Centre, 1/AF, Bidhannagar, Kolkata 700 064, India

An experimental source of neutrons with a wide energy range is optimized using the FLUKA Monte Carlo code. Neutron yield produced by 50 MeV and 100 kW electron beam from a proposed linear accelerator at the Variable Energy Cyclotron Centre, Kolkata is calculated for a thick lead (Pb) target.

Keywords: Electron beam, linear accelerator, Monte Carlo code, optimization calculations, photo-neutron.

PRODUCTION of neutrons through the use of electron beams is well established and has played an important role in neutron experimental physics. The photo-neutron conversion is convenient over other neutron sources such as nuclear reactors. An electron beam can be used to produce bremsstrahlung photons which, in turn, can evoke neutron emission in materials. Many researchers have already studied this method of production of neutrons. Barber and Geoge[1] measured the total neutron yields from thick targets of carbon (C), aluminium (Al), copper (Cu), lead (Pb) and uranium (U) in the range of electron energy from 10 to 36 MeV. Gabriel *et al.*[2] produced neutrons using continuous working (CW) electron linear accelerator (linac) with 1 mA, beam current and 40 MeV beam energy. Bedogni *et al.*[3] have described the photo-neutron source at Frascati National Laboratory, Italy in which an electron beam of 510 MeV was made to fall on a tungsten (W) target inside a polythene–Pb assembly. Kim *et al.*[4] have described Pohang neutron source, in which a 100 MeV electron beam falling on water-cooled tantalum (Ta) target was optimized. This article describes the target optimization study for neutron generation from a thick Pb target with 50 MeV and 100 kW electron beam for the upcoming facility at Advanced National facility for unstable and rare-isotope beams (ANURIB), at Variable Energy Cyclotron Centre (VECC), Kolkata[5]. These photo-neutrons are often utilized for various other purposes such as calibration of instruments, production of radionuclides for use in medical and industrial applications, to name a few.

*For correspondence. (e-mail: nkdas@vecc.gov.in)

Materials and method

The present study was carried out using MC code FLUKA version 2011.2c.3 (refs 6 and 7). The FLUKA code can handle several particle, types including electrons, photons, neutrons and heavy ions in the energy range of a few kilovolts to Tera electronvolt. The PHOTONUC card was used for switching the (γ, n) reaction in the target of interest. In this study, 5×10^7 histories were processed to arrive at the desired statistical convergence (less than 1%) of the output. The geometry of the model used in the simulation was realized with the graphical interface FLAIR[8]. The geometry of the simulation consists of detectors for scoring neutron fluence which were placed at a distance of 10 cm from the centre of the target at 0° and 90° position with respect to the beam direction. The detectors had right circular cylindrical geometries with a radius, of 5.5 cm and height of 1 cm. The material inside the detector has been considered as vacuum in Monte Carlo simulation. Figure 1 shows the geometry used for Monte Carlo (MC) simulation. In this figure, the target is having a radius of 5.5 cm and a thickness of 5.5 cm.

Optimization of target

Choice of target material: When an electron interacts with matter, it loses energy through two processes, viz. collisional loss and radiative loss. Collisional loss, which comprises mainly of ionization and excitation increases logarithmically with energy and linearly with Z (atomic number of the target material). Radiative loss varies linearly with energy and as Z^2. At $E > E_c$, where energy of electron (E) and critical energy of electron (E_c), radiative loss dominates over ionization loss, where E_c is the critical energy. For Pb, $E_c = 9.51$ MeV. As a large part of

the electron energy is dissipated as heat, the target material should be able to withstand heat. Most of the target materials will melt due to high beam current of the accelerator if sufficient cooling arrangements are not made for the target. This heat can be efficiently dissipated through convection in case of liquid targets. The advantage of a liquid target is that the neutron flux is not limited by the heat load of the target. It is limited only by the electron power of the accelerator. Another advantage of the liquid target system is its ability to withstand radiation damage, thus minimizing the waste disposal problem. Moreover, radiation damage to solid targets over a period of time leads to their embrittlement and fracture[9]. This reduces the heat conduction capacity, which in turn affects neutron intensity.

Photonuclear interaction is mainly the result of three specific processes: giant dipole resonance (GDR), quasi-deuteron (QD) production and intra-nuclear cascade. Beyond the threshold energy, the GDR process is dominant in photo-neutron production at energies less than 30 MeV. The (γ, n) reaction energy thresholds are above 7–8 MeV for most high-Z materials. In order for the photo-neutron interaction to occur, the threshold energy (neutron separation energy) must be overcome. So, photo-neutron production is primarily governed by the neutron separation energy and the photo-neutron cross-section. For Pb, this threshold energy is 7.5 MeV. This indicates that at photon energies below 10 MeV, Pb is capable of producing neutrons. However, at higher energies (>15 MeV) it is even capable of producing neutrons through (γ, x_n) reaction[10]. This allows generation of more neutrons with a higher energy electron beam. Pb has a small neutron capture cross-section. Hence, it does not become radioactive and unstable. Based on all these facts, Pb ($Z = 82$) in molten form was chosen as a suitable target material having its melting point ≈327°C. It is non-corrosive and does not dissolve or amalgamate with other materials, the material of the structural container in particular. Another element like tungsten (W) could have been a suitable choice owing to its high atomic number and similar photo-neutron cross-section, but the melting point of W is 3422°C, which makes it unsuitable for liquid targets. W is the appropriate choice for solid targets only. A similar arrangement has been used with Pb for the neutron source at electron linac for beams with high brilliance and low emittance (ELBE) at Forschungszentrum Dresden-Rossendorf, Germany[11].

Size of target: The thickness of the target should be sufficient to be able to stop the primary electron beam completely and should yield maximum photons. The continuous slowing down approximation (CSDA) range of electrons in Pb from ESTAR database is 14.63 g/cm^2 (ref. 12). So, to stop the primary electron beam of 50 MeV, the target should be more than 0.9 cm. The bremsstrahlung photons produced have anisotropic distribution, which is forward-peaked. The Pb target, with cylindrical geometry, was chosen for simulation, with the same radius and thickness. In this study, the target size was varied from $5X_0$ through $20X_0$, where X_0 is the radiation length of electron in Pb (≈0.55 cm). The neutron and photon yields were evaluated in both 0° and 90° positions with respect to the primary electron beam direction. Although the bremsstrahlung photons are forward-peaked, the photo-neutron production through GDR is isotropic in nature. The neutrons at the 90° position would have lower photon contamination.

Results and discussion

The photo-neutron cross-section shown in Figure 2 has been evaluated with TALYS code version 1.8 (ref. 13). The cross-section shows an increasing trend beyond the threshold energy and peaks around ≈15 MeV, thereafter it decreases.

Figure 3 shows the neutron yield (cm^{-2}) per unit primary electron with variation of target size in terms of X_0 at

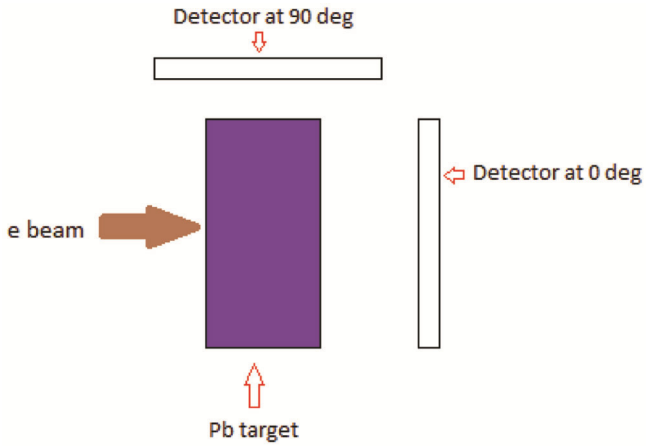

Figure 1. Geometry used for Monte Carlo simulation.

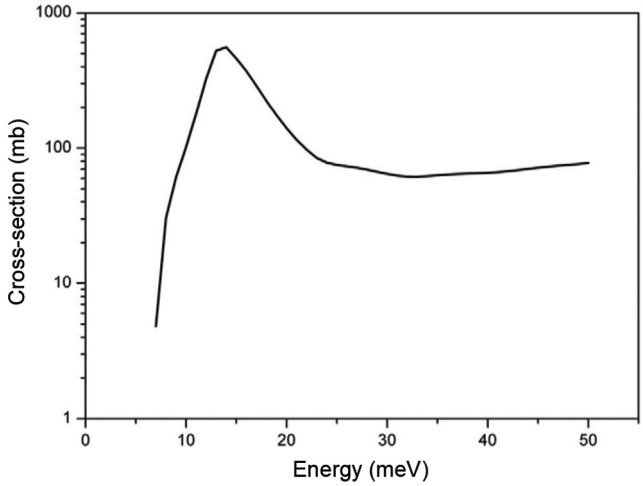

Figure 2. Cross-section of (γ, x_n) reaction for Nat. Pb.

0° and 90° positions with respect to the electron beam direction. For the 0° position, there is a continuous increase in neutron yield up to $17.5X_0$, beyond which it decreases. At the 90° position, neutron yield increases rapidly till $10X_0$ and thereafter increases slowly until $12.5X_0$, beyond which the yield begins to decrease. As the bremsstrahlung photons are forward-peaked, more photons are available for photonuclear interactions at the forward direction. Beyond the peak yield of neutrons, its production decreases due to decrease in the photon yield by virtue of the target itself. Figure 4 shows the photon yield (cm^{-2}) per unit primary electron at 0° and 90° positions with variation of target size in terms of X_0. We can see a marked difference in photon yield at the two positions. In both cases, photon yield decreases with increasing target size. For all target sizes, photon yield is always maximum at 0° position. As photons produced through bremsstrahlung contain both high-energy and low-energy components, an increase in the size of the target attenuates the low-energy components. Hence there is a decrease in photon yield with an increase in the size of the target. However, with photon contamination being less at the 90° position, the target was optimized for $12.5X_0$. Neutron yield at the 90° detector position was found to be 1.72×10^{13} n/s. Although there are no data in the literature for neutron yield from photo-neutron source using 50 MeV accelerator, data from the ELBE photo-neutron source with 40 MeV energy and 1 mA beam current have been compared[11]. The neutron yield obtained with them is 2.7×10^{13} n/s. It is important to understand that the neutron yield is sensitive to energy of the electron beam from the accelerator.

Table 1 shows the ratio of neutron to photon yield at 0° and 90° positions with respect to primary electron beam direction for different target sizes in terms of X_0. It can be seen that for the 0° and 90° positions, the ratio increases with increase in target thickness. The constant increase at the 90° position is mainly due to decrease in the photon yield rather than increase in the neutron yield. So, the optimized thickness of the target was kept at $12.5X_0$.

Figure 5 shows the lethargy plot of the neutron energy spectrum at the 90° position. This energy spectrum has

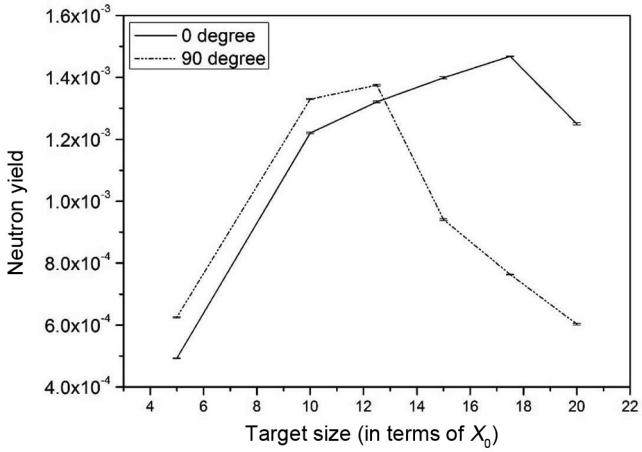

Figure 3. Neutron yield at 0° and 90° positions with different target sizes.

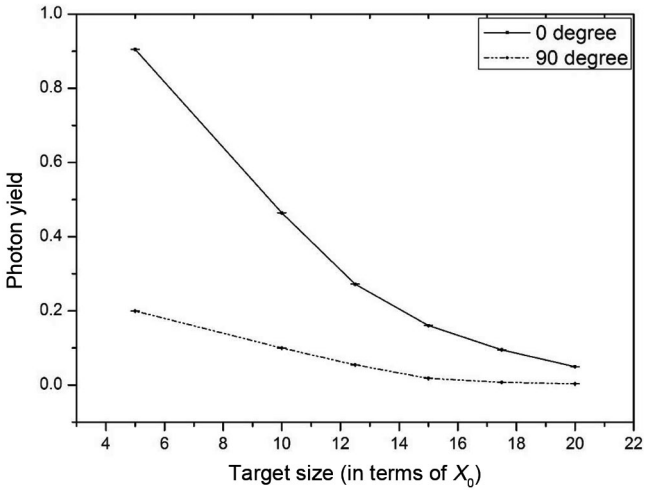

Figure 4. Photon yield at 0° and 90° positions with different target sizes.

Table 1. Ratio of the neutron to photon yield at two positions for various target thickness values

Target size (in terms of X_0)	Ratio of neutron to photon yield at	
	0°	90°
5	5.45E-04	3.14E-03
10	2.63E-03	1.33E-02
12.5	4.85E-03	2.53E-02
15	8.73E-03	5.16E-02
17.5	1.55E-02	1.02E-01
20	2.52E-02	1.94E-01

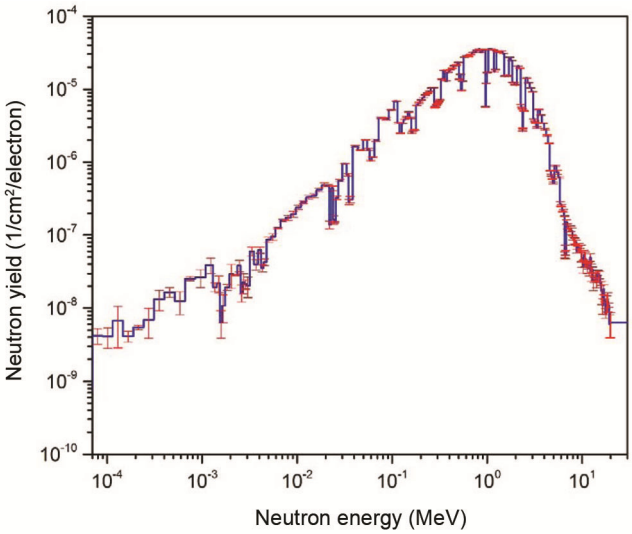

Figure 5. Neutron spectrum at 90° position for target size of $12.5X_0$.

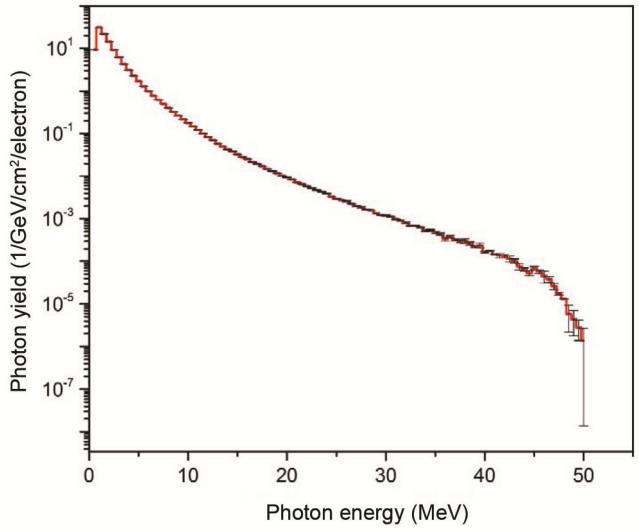

Figure 6. Photon spectrum at 90° position for target size of $12.5X_0$.

been evaluated with 50 MeV electrons impinging on the optimized target thickness of $12.5X_0$. It shows the neutron evaporation peak at ≈1.0 MeV produced mainly through GDR.

Figure 6 shows the semi-log plot of the photon energy spectrum at the 90° position for target size of $12.5X_0$. The energy spectrum of bremsstrahlung photons is continuous with a domination of low energies.

Conclusion

The obtained results of simulations indicate that the largest number of neutrons can be generated in a single high-Z converter like lead when optimal converter thickness is in the range 6–7 cm corresponding to a 50 MeV electron beam. It is observed that the flux of photons decreases as a function of thickness of the converter, while for neutrons the flux increases with thickness to the tune of $12.5X_0$ and then decreases. The photo-neutron energy spectrum peaks at 1 MeV and then decreases.

1. Barber, W. C. and George, W. D., Neutron yields from targets bombarded by electrons. *Phys. Rev*., 1959, **116**(6), 1551–1559.
2. Gabriel, F. *et al.*, The Rossendorf radiation source ELBE and its FEL projects. *Nucl. Instrum. Methods Phys. Res. Sect. B*, 2000, **161–163**, 1143–1147.
3. Bedogni, R., Quintieri, L., Buonomo, B., Esposito, A., Mazzitelli, G., Foggetta, L. and Gómez-Ros, J. M., Experimental and numerical characterization of the neutron field produced in the n@BTFFrascati photo-neutron source. *Nucl. Instru. Methods Phys. Res. Sect. A*, 2011, **659**(1), 373–377.
4. Kim, G. N. *et al*., Measurement of photoneutron spectrum at Pohang neutron facility. *Nucl. Instrum. Methods Phys. Res. Sect. A*, 2002, **485**(3), 458–467.
5. Chakrabarti, A., Bandyopadhyay, A., Naik, V., Dechoudhury, S., Mondal, M. and Nabhiraj, P. Y., The ANURIB project at VECC – plans and preparations. *Nucl. Instrum. Methods Phys. Res. Part B*, 2013, **317**, 253–256.
6. Bohlen, T. T. *et al.*, The FLUKA code: developments and challenges for high energy and medical applications. *Nucl. Data Sheets*, 2014, **120**, 211–214.
7. Ferrari, A., Sala, P. R., Fassò, A. and Ranft, J., FLUKA: a multi-particle transport code. CERN-2005-10, INFN/TC_05/11, SLAC-R-773, 2005.
8. Vlachoudis, V., FLAIR: a powerful but user friendly graphical interface for FLUKA. In Proceedings of International Conference on Mathematics. Computational Methods and Reactor Physics, Saratoga Springs, New York, USA, 2009.
9. Ullmaier, H. and Carsughi, F., Radiation damage problems in high power spallation neutron sources. *Nucl. Instrum. Meth. Phys. Res. Part B*, 1995, **101**, 406–421.
10. Chadwick, M. B. *et al.*, *Handbook on Photonuclear Data for Applications: Cross Sections and Spectra*, *IAEA TECH-DOC*, 2000, p. 1178.
11. Altstadt, E. *et al.*, A photo-neutron source for time-of-flight measurements at the radiation source ELBE. *Ann. Nucl. Energy*, 2007, **34**, 35–50.
12. Berger, M. J., ESTAR, PSTAR and ASTAR: computer programs for calculating stopping powers and ranges for electrons, protons and helium ions, Technical Report, IAEA-TECDOC-799, 1995.
13. Koning, A. J. and Rochman, D., Modern nuclear data evaluation with the TALYS code system. *Nuclear Data Sheets*, 2012, **113**(12), 2841–2934.

ACKNOWLEDGEMENT. We thank the Director, VECC, Kolkata for his keen interest in this research work.

Received 4 April 2019; revised accepted 31 August 2020

doi: 10.18520/cs/v119/i9/1499-1502